ACS APPLIED MATERIALS & INTERFACES

Research Article

www.acsami.org

Rational Design of Bi_2Te_3 Polycrystalline Whiskers for Thermoelectric Applications

Guang Han,[†] Zhi-Gang Chen,*[,†] Lei Yang,[†] Min Hong,[†] John Drennan,[‡] and Jin Zou*[,†,‡]

[†]Materials Engineering and [‡]Centre for Microscopy and Microanalysis, The University of Queensland, Brisbane QLD 4072, Australia

Supporting Information

ABSTRACT: Bi_2Te_3 polycrystalline whiskers consisting of interconnected nanoplates have been synthesized through chemical transformation from In_2Te_3 polycrystalline whisker templates assembled by nanoparticles. The synthesized Bi_2Te_3 whiskers preserve the original one-dimensional morphology of the In_2Te_3, while the In_2Te_3 nanoparticles can be transformed into the Bi_2Te_3 thin nanoplates, accompanied by the formation of high-density interfaces between nanoplates. The hot-pressed nanostructures consolidated from Bi_2Te_3 polycrystalline whiskers at 400 °C demonstrate a promising figure of merit (ZT) of 0.71 at 400 K, which can be attributed to their low thermal conductivity and relatively high electrical conductivity. The small nanoparticles inherited from the polycrystalline whiskers and high-density nanoparticle interfaces in the hot-pressed nanostructures contribute to the significant reduction of thermal conductivity. This study provides a rational chemical transformation approach to design and synthesize polycrystalline microstructures for enhanced thermoelectric performances.

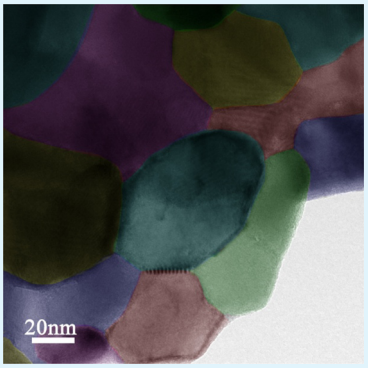

KEYWORDS: *Bi_2Te_3, chemical transformation, thermoelectric, polycrystalline whisker, interface, In_2Te_3*

1. INTRODUCTION

The ever-growing global energy demand has attracted extensive attention to sustainable energy generation and conversion.[1,2] Thermoelectric materials, which can realize the direct conversion from thermal energy to electricity, provide opportunities to harvest useful electricity from waste heat. Therefore, thermoelectric energy conversion is considered to be a promising technique to alleviate global energy demand. The thermoelectric efficiency of a material is determined by its figure of merit (ZT), $ZT = S^2\sigma T/\kappa$ ($\kappa = \kappa_e + \kappa_L$), where S, σ, T, and κ are the Seebeck coefficient, electrical conductivity, absolute temperature, and thermal conductivity (κ_e and κ_L are the electronic and lattice thermal conductivity), respectively.[1−9] The electrical and thermal components in ZT are correlated, which restricts the maximum ZT values of various bulk thermoelectric materials to ∼1 during the past few decades.[1] In recent years, nanostructuring has been proved to be an effective approach to the ZT enhancement, as interfaces introduced by nanostructuring can effectively enhance phonon scattering while less influence carrier transport, leading to significant decrease of κ_L without much influence on electrical properties.[1,2,5,7−12]

Recently, nanostructured bulk materials consolidated directly by nanostructures, such as Bi_2Te_3-based,[13−27] PbTe-based,[28−31] Ag_2Te-based,[32−34] $AgBiSe_2$,[35] $AgBiS_2$,[36] and I_2−II−IV−VI_4 nanostructures,[37−40] synthesized by bottom-up chemical solution methods, have received much attention, due to the effective control on size, morphology, and crystal structure of thermoelectric nanostructures. Especially, great success has been achieved in Bi_2Te_3-based materials, which are promising thermoelectric materials for power generation and refrigeration at room temperature. With extensive effort being devoted to controllable synthesis of Bi_2Te_3-based nanostructures, several excellent morphologies have been developed in enhancing their thermoelectric performances, such as nanoplates/nanosheets,[13−18] ultrathin nanostructures,[19,20] nanoscale heterostructures,[21−24] and one-dimensional nanostructures.[25−27] Specifically, theoretical predictions[41] and experimental measurements[42] indicate that one-dimensional nanostructures, such as nanowires, can enhance the power factor ($S^2\sigma$) due to quantum confinement[41] and achieve low κ_L due to the phonon scattering at the nanostructure surface,[42] which can lead to improved ZT.[41−43] Polycrystalline one-dimensional nanostructures are anticipated to have even lower κ_L than their single crystalline counterparts, due to extra phonon scattering by nanoparticle interfaces within the nanostructures.[26,44] Currently, the solution synthesis of polycrystalline one-dimensional Bi_2Te_3 nanostructures mainly focuses on nanotubes.[26,45,46] However, the low thermal conductivity of such polycrystalline nanotubes was compromised by the relatively low electrical conductivity.[26] Therefore, it is vital to develop a new synthetic method to synthesize polycrystalline one-dimensional Bi_2Te_3 nanostructures with well-controlled components and high-density interfaces, while having simultaneously low thermal conductivity and high electrical conductivity.

In this study, we report a new chemical transformation methodology to fabricate Bi_2Te_3 polycrystalline whiskers from an In_2Te_3 polycrystalline whisker template. The solubility of

Received: November 10, 2014
Accepted: December 12, 2014
Published: December 12, 2014

DOI: 10.1021/am5078528
ACS Appl. Mater. Interfaces 2015, 7, 989−995

Bi_2Te_3 in polar solvents (e.g., ethylene glycol) is lower than that of In_2Te_3,[47] which can lead to a thermodynamic favorable transformation from In_2Te_3 to Bi_2Te_3. Scheme 1 illustrates the potential chemical transformation from In_2Te_3 to Bi_2Te_3 in solution. As can be seen, the (111) planar arrangement of Te in In_2Te_3 (note that In_2Te_3 has a cubic crystal structure with a lattice parameter of a = 18.486 Å)[48] is similar to the (0001) planar arrangement of Te in Bi_2Te_3 (note that Bi_2Te_3 has a rhombohedral crystal structure with lattice parameters of a = 4.386 Å, and c = 30.497 Å),[48] and the adjacent interatomic distance of Te in In_2Te_3 (4.357 Å) is very close to that in Bi_2Te_3 (4.386 Å). Such a close structure relationship between In_2Te_3 and Bi_2Te_3 is anticipated to preserve the general morphology of the In_2Te_3 template in the transformed product and to favor the formation of a single-phase product.[49,50]

Scheme 1. Schematic Structure Illustration of the Proposed Chemical Transformation from In_2Te_3 to Bi_2Te_3 in Solution

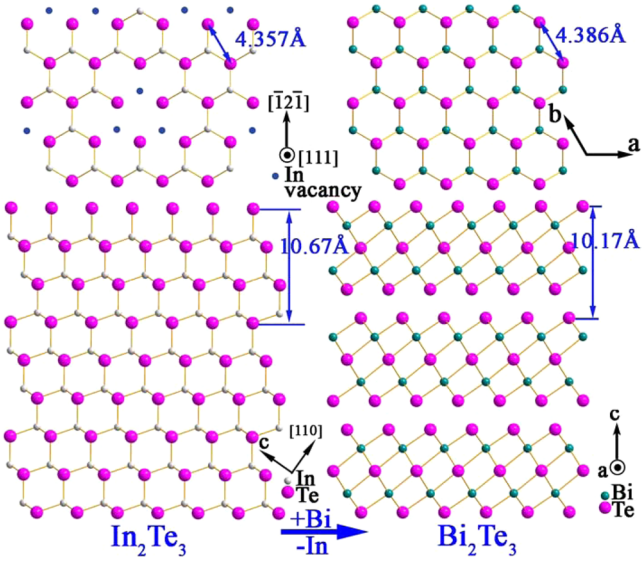

Herein, on the basis of the proposed synthetic approach, we realized the rational synthesis of Bi_2Te_3 polycrystalline whiskers consisting of thin nanoplates. Besides, we studied the thermoelectric property of the hot-pressed nanostructures consolidated by such whiskers, in order to understand the influence of polycrystalline whisker morphology on their thermoelectric performances.

2. EXPERIMENTAL SECTION

Materials Synthesis. In a typical synthesis of In_2Te_3 whiskers, 0.4 mmol of $InCl_3{\cdot}4H_2O$, 0.3 mmol of Na_2TeO_3, 0.2 g of polyvinylpyrrolidone, and 0.2 g of ascorbic acid were added into 50 mL of ethylene glycol. After being stirred for 20 min, the solution was transferred into a Teflon-lined autoclave that was then sealed and annealed at 220 °C for 48 h. After the autoclave was cooled to room temperature naturally, the synthesized products were collected, centrifuged, and washed with deionized water and ethanol several times, and then dried at room temperature.

Bi_2Te_3 polycrystalline whiskers were synthesized by chemical transformation from the synthesized In_2Te_3 whiskers. In a typical synthesis, 10 mg of In_2Te_3 whiskers, 10.3 mg of $BiCl_3$, and 20 mg of ethylenediaminetetraacetic acid were added into 50 mL of ethylene

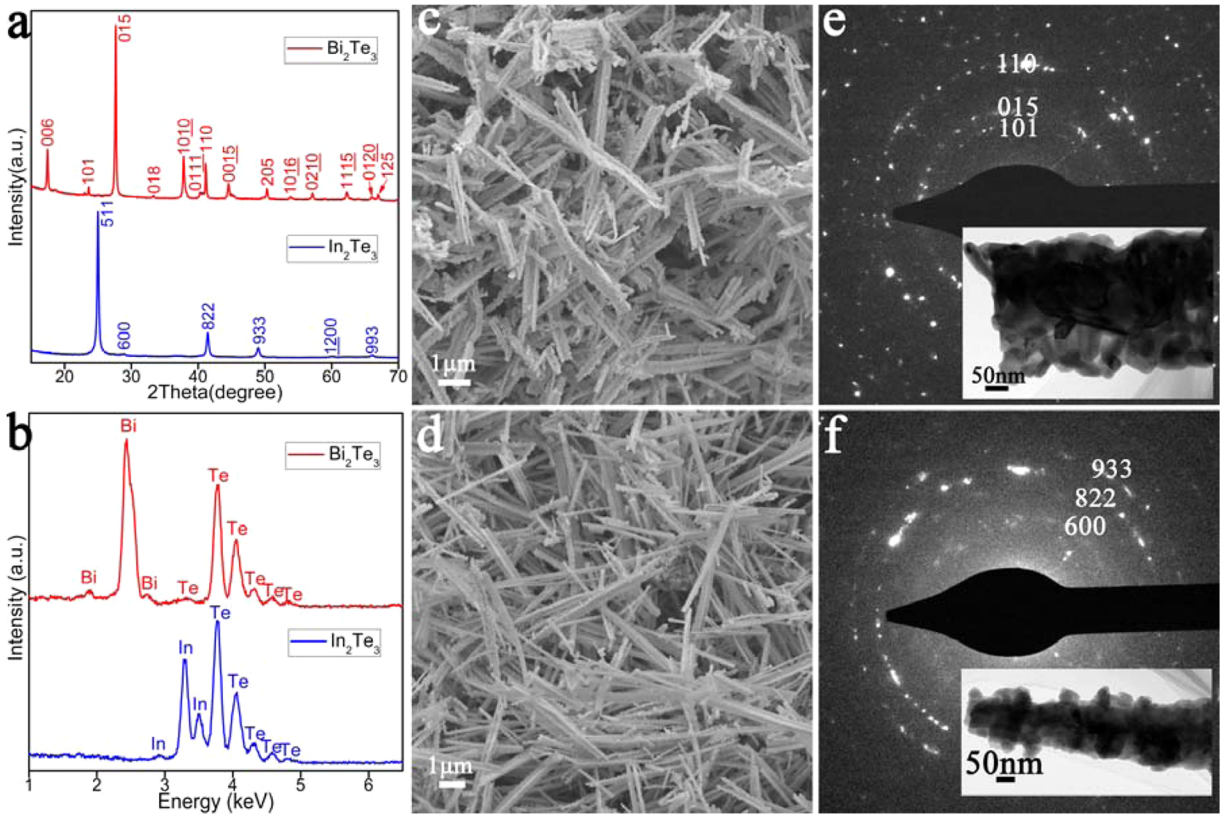

Figure 1. Characterization of the Bi_2Te_3 whiskers through chemical transformation and the In_2Te_3 whiskers via solvothermal synthesis: (a) XRD patterns, (b) EDS spectra, and SEM images of (c) the In_2Te_3 whiskers and (d) the Bi_2Te_3 whiskers and (e and f) SAED patterns of the Bi_2Te_3 whiskers (inset in e) and the In_2Te_3 whiskers (inset in f).

DOI: 10.1021/am5078528
ACS Appl. Mater. Interfaces 2015, 7, 989−995

glycol. After being stirred for 30 min, the solution was transferred into a Teflon-lined autoclave, which was then sealed and annealed at 200 °C for 24 h. The collecting and cleaning process of the Bi_2Te_3 nanostructures is the same as that of the In_2Te_3 nanostructures.

Materials Characterizations. The crystal structures of the synthesized products were determined by X-ray diffraction (XRD, Bruker D8 Advance X-ray diffractometer, Cu Kα radiation with an X-ray wavelength of 1.5418 Å). The morphologies of the synthesized nanostructures were investigated by scanning electron microscopy (SEM, JEOL 7800, operated at 5 kV), and their structural and chemical characteristics were characterized by transmission electron microscopy (TEM, FEI Tecnai F20, operated at 200 kV) equipped with energy-dispersive X-ray spectroscopy (EDS) for compositional analysis.

Thermoelectric Performance Measurement. Bi_2Te_3 powders were hot-pressed into pellets at 400 or 350 °C for 30 min under a vacuum with a uniaxial pressure of 40 MPa. To avoid the influence of nanoplate orientation on the thermoelectric property of the synthesized Bi_2Te_3, the measurements for σ, S, and κ were performed with the samples orientated identically (i.e., perpendicular to the hot-press direction in this study).[16] The σ and S of the Bi_2Te_3 pellets were measured using ULVAC ZEM-3 within the temperature range 300–420 K. The κ of the pellets was calculated through $\kappa = DC_p\rho$, where D, C_p, and ρ are the thermal diffusivity coefficient, specific heat capacity, and density, respectively. D of the Bi_2Te_3 pellets was measured using Netzsch LFA 457 from 300 to 420 K, C_p was measured using Netzsch DSC 404 within the same temperature range, and ρ was calculated by using the mass and dimensions of the pellet. κ_e was estimated by the Wiedemann–Franz law ($\kappa_e = L\sigma T$, where L is the Lorentz number; L of 2.0×10^{-8} V^2 K^{-2} for a degenerate semiconductor was applied in this study),[51] and then, κ_L was calculated using the relationship $\kappa_L = \kappa - \kappa_e$.

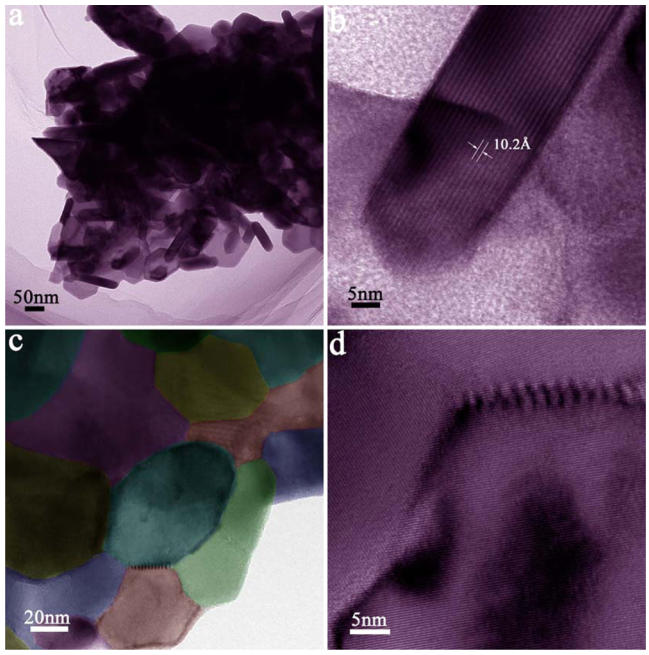

Figure 2. High-magnification TEM images of the Bi_2Te_3 polycrystalline whiskers: (a) typical TEM image showing the general morphology of the whiskers, (b) HRTEM image of a vertical nanoplate, (c) a typical TEM image showing the high-density interfaces within the whiskers (this image was colored to better distinguish the nanoplates), and (d) HRTEM image of the nanoplate interfaces.

3. RESULTS AND DISCUSSION

Figure 1a shows the representative XRD patterns of the products synthesized from chemical transformation of indium tellurides and the original solvothermally produced indium tellurides. As can be seen, the XRD pattern of the products synthesized from chemical transformation can be indexed as the layer-structured rhombohedral Bi_2Te_3 (JCPDS file no. 89-2009), while the indium tellurides obtained through the solvothermal reaction belong to the cubic-structured In_2Te_3 (JCPDS file no. 33-1488).[48] Figure 1b gives the EDS spectra of the synthesized metal tellurides, and strong Bi and Te peaks can be seen for the Bi_2Te_3, while evident In and Te peaks can be observed in the In_2Te_3, both with a metal (Bi or In)/Te atomic ratio of 2:3. Figure 1c and d are the typical SEM images of the Bi_2Te_3 and In_2Te_3, respectively, and show that both metal tellurides are whiskers with lengths of 2–8 μm. Figure 1e and f, as well as their insets, are selected area electron diffraction (SAED) patterns and the corresponding TEM images of the Bi_2Te_3 and In_2Te_3 products. From these, the whiskers can be confirmed to be polycrystals that are composed of small nanoplates and nanoparticles, respectively. Accordingly, In_2Te_3 polycrystalline whiskers have been indeed converted into Bi_2Te_3 polycrystalline whiskers through the chemical transformation.

To further understand the interconnected structural characteristics of the nanoplates, Bi_2Te_3 polycrystalline whiskers were further investigated by TEM. Figure 2a is the typical TEM image of the interconnected nanoplates, and shows the randomly oriented nanoplates. Figure 2b is a high-resolution TEM (HRTEM) image of a vertical nanoplate, and shows a lattice spacing of ~10.2 Å that is consistent with the lattice spacing of the {0003} atomic plane of Bi_2Te_3, suggesting the nanoplate has a thickness of ~20 nm. Figure 2c shows the general morphology of the interconnected Bi_2Te_3 nanoplates, in which Bi_2Te_3 nanoplates build a large amount of interfaces between them. Figure 2d is a representative HRTEM image, and shows differently orientated highly crystalline nanoplates. Besides, on the basis of the TEM statistical analysis, the Bi_2Te_3 nanoplates have a lateral diameter of 40 ± 20 nm and a thickness of 15 ± 5 nm.

To understand the thermoelectric performance of the synthesized Bi_2Te_3 polycrystalline whiskers, detailed thermoelectric evaluation was performed on the samples hot-pressed from the whiskers at 400 °C. Figure 3a presents the temperature-dependent σ of the hot-pressed sample, and reveals that the σ decreases slightly with increasing temperature. The σ peak value of ~57 800 S m^{-1} is much higher than that of reported solution-based Bi_2Te_3, such as polycrystalline nanotubes,[26] nanorod bundles,[25] ultrathin nanowires,[52] and nanostring-cluster structures.[53] Such a promising σ can be attributed to the high crystallinity and preformed a high density of interfaces of Bi_2Te_3 nanoplates in the polycrystalline whiskers, as demonstrated in their structural characteristics (refer to Figure 2). Figure 3b is the variation of S of the Bi_2Te_3 hot-pressed sample as a function of temperature, and shows the negative sign of S, indicating the n-type conducting behavior. A peak value of −153.5 μV K^{-1} is obtained at 400 K, which is comparable to the reported S values for other binary Bi_2Te_3 nanostructures, such as polycrystalline nanotubes,[26] ultrathin nanosheets,[20] mesoporous structures,[54] and nanostring-cluster structures.[53] Figure 3c gives the κ profile of the Bi_2Te_3 as a function of temperature. As can be seen, a very low κ (e.g., 0.74 W m^{-1} K^{-1} at 360 K) has been obtained, which is significantly lower than that of bulk Bi_2Te_3 (1.5–2.5 W m^{-1} K^{-1}).[55] Especially, low κ_L values of 0.3–0.41 W m^{-1} K^{-1} have been obtained over the entire measurement temperature range. To

DOI: 10.1021/am5078528
ACS Appl. Mater. Interfaces 2015, 7, 989–995

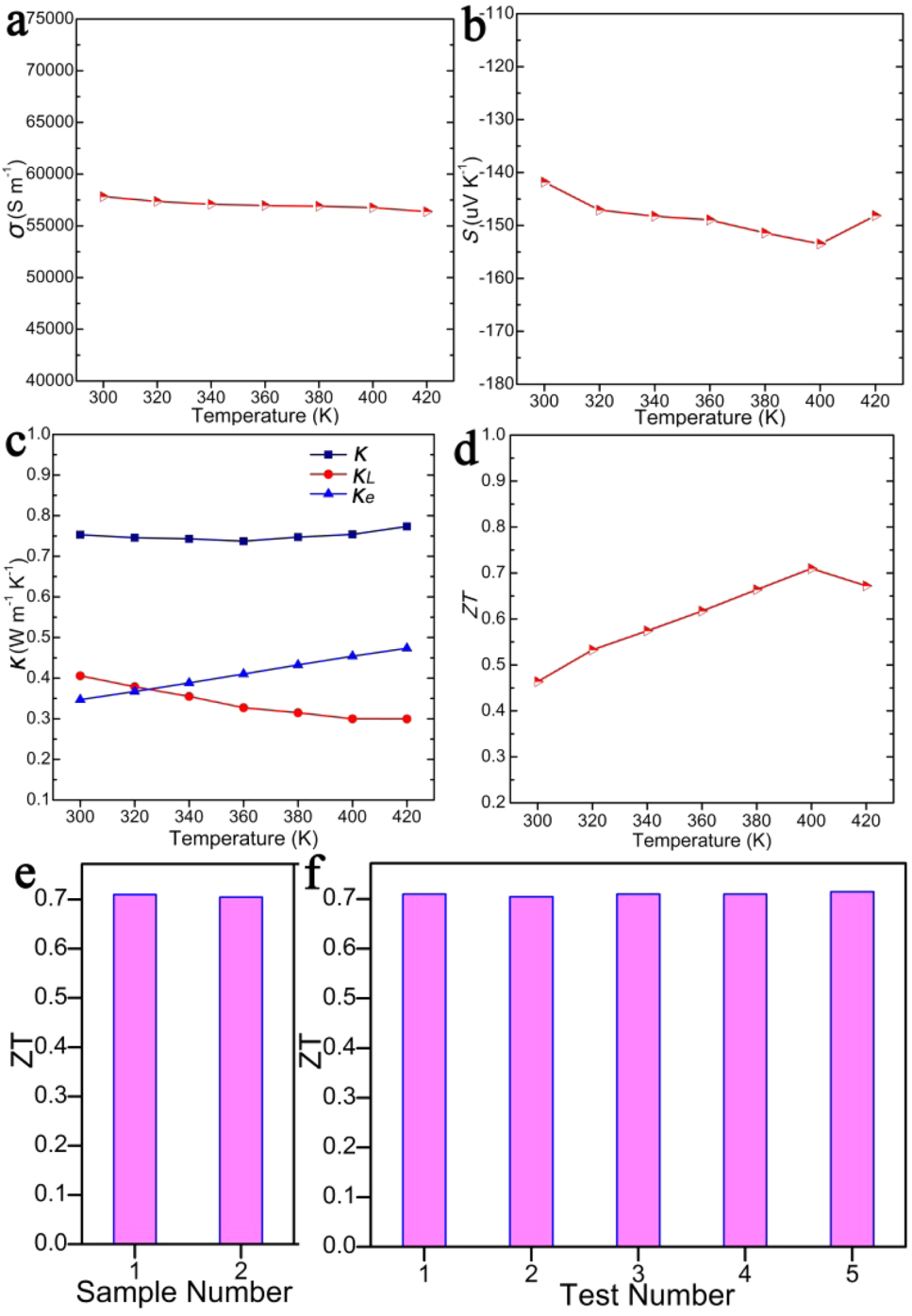

Figure 3. Thermoelectric performances of Bi_2Te_3 pellets hot-pressed from Bi_2Te_3 polycrystalline whiskers at 400 °C: (a) σ, (b) S, (c) κ, (d) ZT, (e) ZT reproducibility, and (f) ZT stability.

understand the reason for the low thermal conductivity, we perform structural characterization on the obtained Bi_2Te_3 hot-pressed nanostructures. Figure 4a is a typical TEM image, and shows that small grains with various orientations and with a high density of interfaces can be retained after the hot-press process. Due to the overlapping of the nanoparticles, the particle interfaces observed by TEM are not as clear as those in the solvothermal whiskers. Figure 4b is the HRTEM image of the nanoparticles, and demonstrates their high crystallinity. Therefore, the small highly crystalline nanoparticles inherited from the polycrystalline whiskers and their corresponding high-density interfaces in the hot-pressed nanostructures can significantly scatter the phonons and contribute to the significant reduction of κ_L.

On the basis of these measurements, the Bi_2Te_3 hot-pressed nanostructures (pressed at 400 °C) exhibit relatively promising ZT (higher than 0.46) over the entire measurement temperature range of 300−420 K, with the maximum ZT reaching 0.71 at 400 K (Figure 3d). This value is higher or comparable to that of other Bi_2Te_3 nanostructures synthesized by various solution-based methods, such as 0.236 for Bi_2Te_3−Te nanowire heterostructures,[21] 0.43 for nanorod bundles,[25] 0.62 for ultrathin nanoplates,[20] 0.7 for mesoporous monoliths,[54] and 0.77 for nanotubes.[27] We anticipate that the unique structural

DOI: 10.1021/am5078528
ACS Appl. Mater. Interfaces 2015, 7, 989−995

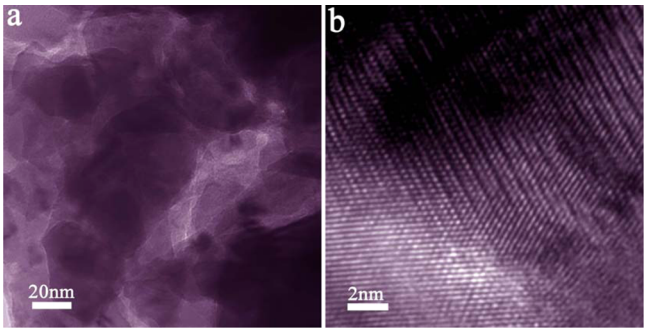

Figure 4. TEM images of the Bi_2Te_3 hot-pressed nanostructures: (a) typical TEM image showing the general morphology of the hot-pressed nanostructures and (b) HRTEM image demonstrating their high crystallinity.

design of the polycrystalline nanostructures, including a small thickness and lateral dimension of the nanoplates, and the high crystallinity with a very high density of interfaces are responsible for the decreased thermal conductivity and enhanced electrical conductivity, which synergistically lead to improved *ZT* values. Moreover, the hot-pressing conditions were adjusted to optimize the thermoelectric properties of the whiskers. The Bi_2Te_3 sample pressed at 350 °C (Figure S1, Supporting Information) obtains a *ZT* value of 0.59 at 400 K, which is inferior to that of the sample pressed at 400 °C (Figure 3). However, the κ of the sample is also significantly reduced compared to the bulk Bi_2Te_3,[55] indicating that the chemical transformation is an effective approach in synthesizing Bi_2Te_3 microstructures with significantly reduced κ.

As reproducibility and stability of thermoelectric performance is an important concern for any nanostructured thermoelectric materials consolidated from solution-synthesized nanomaterials, we measured the *ZT* of another Bi_2Te_3 hot-pressed sample (pressed at 400 °C) from different synthesis batches (Figure 3e) and our first hot-pressed sample in five consecutive evaluations (Figure 3f). It is found that the *ZT* of the Bi_2Te_3 samples stabilizes at a value of ~0.71 at 400 K, indicating their high performance reproducibility and stability. Therefore, it can be concluded that chemical transformation has been demonstrated to be a rational approach to design and synthesize Bi_2Te_3 polycrystalline microstructures for enhanced and stable thermoelectric performances.

4. CONCLUSIONS

Chemical transformation has been applied for the template synthesis of Bi_2Te_3 polycrystalline whiskers consisting of interconnected thin nanoplates from In_2Te_3 polycrystalline whiskers. The hot-pressed nanostructures consolidated from such Bi_2Te_3 polycrystalline whiskers at 400 °C show low thermal conductivity and good electrical conductivity, with a promising *ZT* of 0.71 achieved at 400 K. This chemical transformation strategy reported here can be extended to the design and synthesis of other metal chalcogenide polycrystalline whiskers with potential advanced properties.

■ ASSOCIATED CONTENT

Supporting Information

Figure showing the thermoelectric performances of Bi_2Te_3 pellets hot-pressed from Bi_2Te_3 polycrystalline whiskers at 350 °C. This material is available free of charge via the Internet at http://pubs.acs.org.

■ AUTHOR INFORMATION

Corresponding Authors

*E-mail: j.zou@uq.edu.au.
*E-mail: z.chenz@uq.edu.au.

Notes

The authors declare no competing financial interest.

■ ACKNOWLEDGMENTS

This work was financially supported by the Australian Research Council (DP110100565, DP50100056). Z.-G.C. thanks the QLD government for a smart state future fellowship (2011002414). The Australian Microscopy & Microanalysis Research Facility is acknowledged for providing characterization facilities.

■ REFERENCES

(1) Szczech, J. R.; Higgins, J. M.; Jin, S. Enhancement of the Thermoelectric Properties in Nanoscale and Nanostructured Materials. *J. Mater. Chem.* **2011**, *21*, 4037−4055.
(2) Han, G.; Chen, Z.-G.; Drennan, J.; Zou, J. Indium Selenides: Structural Characteristics, Synthesis and Their Thermoelectric Performances. *Small* **2014**, *10*, 2747−2765.
(3) Sootsman, J. R.; Chung, D. Y.; Kanatzidis, M. G. New and Old Concepts in Thermoelectric Materials. *Angew. Chem., Int. Ed.* **2009**, *48*, 8616−8639.
(4) Tritt, T. M.; Subramanian, M. A. Thermoelectric Materials, Phenomena, and Applications: a Bird's Eye View. *MRS Bull.* **2006**, *31*, 188−194.
(5) Lan, Y.; Minnich, A. J.; Chen, G.; Ren, Z. Enhancement of Thermoelectric Figure-of-Merit by a Bulk Nanostructuring Approach. *Adv. Funct. Mater.* **2010**, *20*, 357−376.
(6) Snyder, G. J.; Toberer, E. S. Complex Thermoelectric Materials. *Nat. Mater.* **2008**, *7*, 105−114.
(7) Dresselhaus, M. S.; Chen, G.; Tang, M. Y.; Yang, R. G.; Lee, H.; Wang, D. Z.; Ren, Z. F.; Fleurial, J. P.; Gogna, P. New Directions for Low-Dimensional Thermoelectric Materials. *Adv. Mater.* **2007**, *19*, 1043−1053.
(8) Chen, Z.-G.; Han, G.; Yang, L.; Cheng, L. N.; Zou, J. Nanostructured Thermoelectric Materials: Current Research and Future Challenge. *Prog. Nat. Sci.: Mater. Int.* **2012**, *22*, 535−549.
(9) Zhao, L. D.; Dravid, V. P.; Kanatzidis, M. G. The Panoscopic Approach to High Performance Thermoelectrics. *Energy Environ. Sci.* **2014**, *7*, 251−268.
(10) Poudel, B.; Hao, Q.; Ma, Y.; Lan, Y.; Minnich, A.; Yu, B.; Yan, X.; Wang, D.; Muto, A.; Vashaee, D.; Chen, X.; Liu, J.; Dresselhaus, M. S.; Chen, G.; Ren, Z. High-Thermoelectric Performance of Nanostructured Bismuth Antimony Telluride Bulk Alloys. *Science* **2008**, *320*, 634−638.
(11) Biswas, K.; He, J.; Zhang, Q.; Wang, G.; Uher, C.; Dravid, V. P.; Kanatzidis, M. G. Strained Endotaxial Nanostructures with High Thermoelectric Figure of Merit. *Nat. Chem.* **2011**, *3*, 160−166.
(12) Biswas, K.; He, J. Q.; Blum, I. D.; Wu, C. I.; Hogan, T. P.; Seidman, D. N.; Dravid, V. P.; Kanatzidis, M. G. High-Performance Bulk Thermoelectrics with All-Scale Hierarchical Architectures. *Nature* **2012**, *489*, 414−418.
(13) Mehta, R. J.; Zhang, Y. L.; Karthik, C.; Singh, B.; Siegel, R. W.; Borca-Tasciuc, T.; Ramanath, G. A New Class of Doped Nanobulk High-Figure-of-Merit Thermoelectrics by Scalable Bottom-Up Assembly. *Nat. Mater.* **2012**, *11*, 233−240.
(14) Soni, A.; Zhao, Y. Y.; Yu, L. G.; Aik, M. K. K.; Dresselhaus, M. S.; Xiong, Q. H. Enhanced Thermoelectric Properties of Solution Grown $Bi_2Te_{3-x}Se_x$ Nanoplatelet Composites. *Nano Lett.* **2012**, *12*, 1203−1209.
(15) Scheele, M.; Oeschler, N.; Veremchuk, I.; Reinsberg, K. G.; Kreuziger, A. M.; Kornowski, A.; Broekaert, J.; Klinke, C.; Weller, H. ZT Enhancement in Solution-Grown $Sb_{2-x}Bi_xTe_3$ Nanoplatelets. *ACS Nano* **2010**, *4*, 4283−4291.

DOI: 10.1021/am5078528
ACS Appl. Mater. Interfaces 2015, 7, 989−995

(16) Min, Y.; Roh, J. W.; Yang, H.; Park, M.; Kim, S. I.; Hwang, S.; Lee, S. M.; Lee, K. H.; Jeong, U. Surfactant-Free Scalable Synthesis of Bi_2Te_3 and Bi_2Se_3 Nanoflakes and Enhanced Thermoelectric Properties of Their Nanocomposites. *Adv. Mater.* **2013**, *25*, 1425−1429.
(17) Zhang, Y.; Hu, L. P.; Zhu, T. J.; Xie, J.; Zhao, X. B. High Yield Bi_2Te_3 Single Crystal Nanosheets with Uniform Morphology via a Solvothermal Synthesis. *Cryst. Growth Des.* **2013**, *13*, 645−651.
(18) Fu, J. P.; Song, S. Y.; Zhang, X. G.; Cao, F.; Zhou, L.; Li, X. Y.; Zhang, H. J. Bi_2Te_3 Nanoplates and Nanoflowers: Synthesized by Hydrothermal Process and Their Enhanced Thermoelectric Properties. *CrystEngComm* **2012**, *14*, 2159−2165.
(19) Zhang, G.; Kirk, B.; Jauregui, L. A.; Yang, H.; Xu, X.; Chen, Y. P.; Wu, Y. Rational Synthesis of Ultrathin n-Type Bi_2Te_3 Nanowires with Enhanced Thermoelectric Properties. *Nano Lett.* **2011**, *12*, 56−60.
(20) Son, J. S.; Choi, M. K.; Han, M. K.; Park, K.; Kim, J. Y.; Lim, S. J.; Oh, M.; Kuk, Y.; Park, C.; Kim, S. J.; Hyeon, T. n-Type Nanostructured Thermoelectric Materials Prepared from Chemically Synthesized Ultrathin Bi_2Te_3 Nanoplates. *Nano Lett.* **2012**, *12*, 640−647.
(21) Zhang, G.; Fang, H.; Yang, H.; Jauregui, L. A.; Chen, Y. P.; Wu, Y. Design Principle of Telluride-Based Nanowire Heterostructures for Potential Thermoelectric Applications. *Nano Lett.* **2012**, *12*, 3627−3633.
(22) Cheng, L.; Chen, Z.-G.; Yang, L.; Han, G.; Xu, H.-Y.; Snyder, G. J.; Lu, G.-Q.; Zou, J. T-Shaped Bi_2Te_3-Te Heteronanojunctions: Epitaxial Growth, Structural Modeling, and Thermoelectric Properties. *J. Phys. Chem. C* **2013**, *117*, 12458−12464.
(23) Mehta, R. J.; Karthik, C.; Singh, B.; Teki, R.; Borca-Tasciuc, T.; Ramanath, G. Seebeck Tuning in Chalcogenide Nanoplate Assemblies by Nanoscale Heterostructuring. *ACS Nano* **2010**, *4*, 5055−5060.
(24) Zhang, Y. C.; Wang, H.; Kraemer, S.; Shi, Y. F.; Zhang, F.; Snedaker, M.; Ding, K. L.; Moskovits, M.; Snyder, G. J.; Stuck, G. D. Surfactant-Free Synthesis of Bi_2Te_3-Te Micro-Nano Heterostructure with Enhanced Thermoelectric Figure of Merit. *ACS Nano* **2011**, *5*, 3158−3165.
(25) Song, S. Y.; Fu, J. P.; Li, X. Y.; Gao, W.; Zhang, H. J. Facile Synthesis and Thermoelectric Properties of Self-assembled Bi_2Te_3 One-Dimensional Nanorod Bundles. *Chem.—Eur. J.* **2013**, *19*, 2889−2894.
(26) Chai, Z.; Wang, H.; Suo, Q.; Wu, N.; Wang, X.; Wang, C. Thermoelectric Metal Tellurides with Nanotubular Structures Synthesized by the Kirkendall Effect and Their Reduced Thermal Conductivities. *CrystEngComm* **2014**, *16*, 3507−3514.
(27) Zhu, H.-T.; Luo, J.; Liang, J.-K. Synthesis of Highly Crystalline Bi_2Te_3 Nanotubes and Their Enhanced Thermoelectric Properties. *J. Mater. Chem. A* **2014**, *2*, 12821−12826.
(28) Fang, H. Y.; Feng, T. L.; Yang, H. R.; Ruan, X. L.; Wu, Y. Synthesis and Thermoelectric Properties of Compositional-Modulated Lead Telluride-Bismuth Telluride Nanowire Heterostructures. *Nano Lett.* **2013**, *13*, 2058−2063.
(29) Finefrock, S. W.; Zhang, G.; Bahk, J.-H.; Fang, H.; Yang, H.; Shakouri, A.; Wu, Y. Structure and Thermoelectric Properties of Spark Plasma Sintered Ultrathin PbTe Nanowires. *Nano Lett.* **2014**, *14*, 3466−3473.
(30) Fang, H.; Luo, Z.; Yang, H.; Wu, Y. The Effects of the Size and the Doping Concentration on the Power Factor of n-type Lead Telluride Nanocrystals for Thermoelectric Energy Conversion. *Nano Lett.* **2014**, *14*, 1153−1157.
(31) Scheele, M.; Oeschler, N.; Veremchuk, I.; Peters, S.-O.; Littig, A.; Kornowski, A.; Klinke, C.; Weller, H. Thermoelectric Properties of Lead Chalcogenide Core−Shell Nanostructures. *ACS Nano* **2011**, *5*, 8541−8551.
(32) Yang, H.; Bahk, J.-H.; Day, T.; Mohammed, A. M. S.; Min, B.; Snyder, G. J.; Shakouri, A.; Wu, Y. Composition Modulation of Ag_2Te Nanowires for Tunable Electrical and Thermal Properties. *Nano Lett.* **2014**, *14*, 5398−5404.
(33) Cadavid, D.; Ibanez, M.; Shavel, A.; Dura, O. J.; Lopez de la Torre, M. A.; Cabot, A. Organic Ligand Displacement by Metal Salts to Enhance Nanoparticle Functionality: Thermoelectric Properties of Ag_2Te. *J. Mater. Chem. A* **2013**, *1*, 4864−4870.
(34) Zhou, W.; Zhao, W.; Lu, Z.; Zhu, J.; Fan, S.; Ma, J.; Hng, H. H.; Yan, Q. Preparation and Thermoelectric Properties of Sulfur Doped Ag_2Te Nanoparticles via Solvothermal Methods. *Nanoscale* **2012**, *4*, 3926−3931.
(35) Xiao, C.; Qin, X.; Zhang, J.; An, R.; Xu, J.; Li, K.; Cao, B.; Yang, J.; Ye, B.; Xie, Y. High Thermoelectric and Reversible p-n-p Conduction Type Switching Integrated in Dimetal Chalcogenide. *J. Am. Chem. Soc.* **2012**, *134*, 18460−18466.
(36) Guin, S. N.; Biswas, K. Cation Disorder and Bond Anharmonicity Optimize the Thermoelectric Properties in Kinetically Stabilized Rocksalt $AgBiS_2$ Nanocrystals. *Chem. Mater.* **2013**, *25*, 3225−3231.
(37) Ibáñez, M.; Zamani, R.; Gorsse, S.; Fan, J.; Ortega, S.; Cadavid, D.; Morante, J. R.; Arbiol, J.; Cabot, A. Core−Shell Nanoparticles as Building Blocks for the Bottom-Up Production of Functional Nanocomposites: PbTe−PbS Thermoelectric Properties. *ACS Nano* **2013**, *7*, 2573−2586.
(38) Fan, F. J.; Wang, Y. X.; Liu, X. J.; Wu, L.; Yu, S. H. Large-Scale Colloidal Synthesis of Non-Stoichiometric $Cu_2ZnSnSe_4$ Nanocrystals for Thermoelectric Applications. *Adv. Mater.* **2012**, *24*, 6158−6163.
(39) Fan, F.-J.; Yu, B.; Wang, Y.-X.; Zhu, Y.-L.; Liu, X.-J.; Yu, S.-H.; Ren, Z. Colloidal Synthesis of $Cu_2CdSnSe_4$ Nanocrystals and Hot-Pressing to Enhance the Thermoelectric Figure-of-Merit. *J. Am. Chem. Soc.* **2011**, *133*, 15910−15913.
(40) Ibáñez, M.; Zamani, R.; LaLonde, A.; Cadavid, D.; Li, W.; Shavel, A.; Arbiol, J.; Morante, J. R.; Gorsse, S.; Snyder, G. J.; Cabot, A. $Cu_2ZnGeSe_4$ Nanocrystals: Synthesis and Thermoelectric Properties. *J. Am. Chem. Soc.* **2012**, *134*, 4060−4063.
(41) Hicks, L. D.; Dresselhaus, M. S. Thermoelectric Figure of Merit of a One-Dimensional Conductor. *Phys. Rev. B* **1993**, *47*, 16631−16634.
(42) Hochbaum, A. I.; Chen, R. K.; Delgado, R. D.; Liang, W. J.; Garnett, E. C.; Najarian, M.; Majumdar, A.; Yang, P. D. Enhanced Thermoelectric Performance of Rough Slicon Nanowires. *Nature* **2008**, *451*, 163−167.
(43) Tan, M.; Deng, Y.; Wang, Y. Ordered Structure and High Thermoelectric Properties of $Bi_2(Te,Se)_3$ nanowire array. *Nano Energy* **2014**, *3*, 144−151.
(44) Moore, A. L.; Pettes, M. T.; Zhou, F.; Shi, L. Thermal Conductivity Suppression in Bismuth Nanowires. *J. Appl. Phys.* **2009**, *106*, 7.
(45) Chai, Z.; Peng, Z.; Wang, C.; Zhang, H. Synthesis of Polycrystalline Nanotubular Bi_2Te_3. *Mater. Chem. Phys.* **2009**, *113*, 664−669.
(46) Xiao, F.; Yoo, B.; Lee, K. H.; Myung, N. V. Synthesis of Bi_2Te_3 Nanotubes by Galvanic Displacement. *J. Am. Chem. Soc.* **2007**, *129*, 10068−10069.
(47) Moon, G. D.; Ko, S.; Min, Y.; Zeng, J.; Xia, Y. N.; Jeong, U. Chemical Transformations of Nanostructured Materials. *Nano Today* **2011**, *6*, 186−203.
(48) PDF-2 Release 2008, Joint Committee on Powder Diffraction Standards (JCPDS)-International Centre for Diffraction Data (ICDD): 2008.
(49) Moon, G. D.; Ko, S.; Xia, Y. N.; Jeong, U. Chemical Transformations in Ultrathin Chalcogenide Nanowires. *ACS Nano* **2010**, *4*, 2307−2319.
(50) Han, G.; Chen, Z.-G.; Ye, D.; Yang, L.; Wang, L.; Drennan, J.; Zou, J. In-Doped Bi_2Se_3 Hierarchical Nanostructures as Anode Materials for Li-Ion Batteries. *J. Mater. Chem. A* **2014**, *2*, 7109−7116.
(51) Sales, B. C.; Mandrus, D.; Chakoumakos, B. C.; Keppens, V.; Thompson, J. R. Filled Skutterudite Antimonides: Electron Crystals and Phonon Glasses. *Phys. Rev. B* **1997**, *56*, 15081−15089.
(52) Wang, K.; Liang, H.-W.; Yao, W.-T.; Yu, S.-H. Templating Synthesis of Uniform Bi_2Te_3 Nanowires with High Aspect Ratio in Triethylene Glycol (TEG) and Their Thermoelectric Performance. *J. Mater. Chem.* **2011**, *21*, 15057−15062.

DOI: 10.1021/am5078528
ACS Appl. Mater. Interfaces 2015, 7, 989−995

(53) Mi, J.-L.; Lock, N.; Sun, T.; Christensen, M.; Søndergaard, M.; Hald, P.; Hng, H. H.; Ma, J.; Iversen, B. B. Biomolecule-Assisted Hydrothermal Synthesis and Self-Assembly of Bi_2Te_3 Nanostring-Cluster Hierarchical Structure. *ACS Nano* **2010**, *4*, 2523−2530.
(54) Zhang, Y. C.; Day, T.; Snedaker, M. L.; Wang, H.; Kramer, S.; Birkel, C. S.; Ji, X. L.; Liu, D. Y.; Snyder, G. J.; Stucky, G. D. A Mesoporous Anisotropic n-Type Bi_2Te_3 Monolith with Low Thermal Conductivity as an Efficient Thermoelectric Material. *Adv. Mater.* **2012**, *24*, 5065−5070.
(55) Kaibe, H.; Tanaka, Y.; Sakata, M.; Nishida, I. Anisotropic Galvanomagnetic and Thermoelectric Properties of n-type Bi_2Te_3 Single Crystal with the Composition of a Useful Thermoelectric Cooling Material. *J. Phys. Chem. Solids* **1989**, *50*, 945−950.

DOI: 10.1021/am5078528
ACS Appl. Mater. Interfaces 2015, 7, 989−995